Biomedical Optics EXPRESS

Virtual optical biopsy of human adipocytes with third harmonic generation microscopy

Cheng-Kun Tsai,[1] Tzung-Dau Wang,[2,3,4,6] Jong-Wei Lin,[2] Ron-Bin Hsu,[5] Lun-Zhang Guo,[1] San-Tai Chen,[1] and Tzu-Ming Liu[1,4,7]

[1]*Institute of Biomedical Engineering, National Taiwan University, Taipei 10617, Taiwan*
[2]*Division of Cardiology, Department of Internal Medicine, National Taiwan University Hospital and National Taiwan University College of Medicine, Taipei 10617, Taiwan*
[3]*Cardiovascular Center and Department of Internal Medicine, National Taiwan University Hospital Yun-Lin Branch, Yun-Lin County 64041, Taiwan*
[4]*Molecular Imaging Center, National Taiwan University, Taipei 10617, Taiwan*
[5]*Department of Surgery, National Taiwan University Hospital, Taipei 10048, Taiwan*
[6]*tdwang@ntu.edu.tw*
[7]*tmliu@ntu.edu.tw*

Abstract: Using the sectioning capability of third harmonic generation (THG) microscopy, we assessed the morphologic features of human adipocytes directly without fixation and labeling. At the plane of the largest cross-sectional area, both area-equivalent circular diameters (AECD) and perimeters of adipocytes were measured, and their statistical distributions were examined. We found, in patients with no cardiovascular risk factors, the average AECD of epicardial adipocytes were 70–90 μm with 11–17 μm standard deviations. In contrast, for patients with coronary artery disease, amounts of small-sized (AECD <40 μm) epicardial adipocytes were observed and the corresponding standard deviations of AECD were increased to 20–29 μm. Our results indicate that the THG tomography platform can be used to explore the histopathological features of adipocytes in clinical scenarios based on its superior resolution for virtual optical biopsy.

OCIS codes: (170.6900) Three-dimensional microscopy; (190.1900) Diagnostic applications of nonlinear optics.

References and links

1. P. Wang, E. Mariman, J. Keijer, F. Bouwman, J. P. Noben, J. Robben, and J. Renes, "Profiling of the secreted proteins during 3T3-L1 adipocyte differentiation leads to the identification of novel adipokines," Cell. Mol. Life Sci. **61**(18), 2405–2417 (2004).
2. H. Hauner, "Secretory factors from human adipose tissue and their functional role," Proc. Nutr. Soc. **64**(02), 163–169 (2005).
3. G. Fantuzzi, "Adipose tissue, adipokines, and inflammation," J. Allergy Clin. Immunol. **115**(5), 911–919, quiz 920 (2005).
4. J. P. Bastard, M. Maachi, C. Lagathu, M. J. Kim, M. Caron, H. Vidal, J. Capeau, and B. Feve, "Recent advances in the relationship between obesity, inflammation, and insulin resistance," Eur. Cytokine Netw. **17**(1), 4–12 (2006).
5. M. Dolinková, I. Dostálová, Z. Lacinová, D. Michalský, D. Haluzíková, M. Mráz, M. Kasalický, and M. Haluzík, "The endocrine profile of subcutaneous and visceral adipose tissue of obese patients," Mol. Cell. Endocrinol. **291**(1-2), 63–70 (2008).
6. G. S. Hotamisligil, P. Arner, J. F. Caro, R. L. Atkinson, and B. M. Spiegelman, "Increased adipose tissue expression of tumor necrosis factor-alpha in human obesity and insulin resistance," J. Clin. Invest. **95**(5), 2409–2415 (1995).
7. P. Mathieu, P. Pibarot, E. Larose, P. Poirier, A. Marette, and J. P. Després, "Visceral obesity and the heart," Int. J. Biochem. Cell Biol. **40**(5), 821–836 (2008).
8. B. L. Wajchenberg, "Subcutaneous and visceral adipose tissue: their relation to the metabolic syndrome," Endocr. Rev. **21**(6), 697–738 (2000).
9. K. E. Wellen and G. S. Hotamisligil, "Obesity-induced inflammatory changes in adipose tissue," J. Clin. Invest. **112**(12), 1785–1788 (2003).

#177650 - $15.00 USD Received 8 Oct 2012; revised 19 Nov 2012; accepted 21 Nov 2012; published 20 Dec 2012

10. P. Björntorp, ""Portal" adipose tissue as a generator of risk factors for cardiovascular disease and diabetes," Arteriosclerosis **10**(4), 493–496 (1990).
11. J. N. Fain, A. K. Madan, M. L. Hiler, P. Cheema, and S. W. Bahouth, "Comparison of the release of adipokines by adipose tissue, adipose tissue matrix, and adipocytes from visceral and subcutaneous abdominal adipose tissues of obese humans," Endocrinology **145**(5), 2273–2282 (2004).
12. S. P. Weisberg, D. McCann, M. Desai, M. Rosenbaum, R. L. Leibel, and A. W. Ferrante, Jr., "Obesity is associated with macrophage accumulation in adipose tissue," J. Clin. Invest. **112**(12), 1796–1808 (2003).
13. S. Eroglu, L. E. Sade, A. Yildirir, U. Bal, S. Ozbicer, A. S. Ozgul, H. Bozbas, A. Aydinalp, and H. Muderrisoglu, "Epicardial adipose tissue thickness by echocardiography is a marker for the presence and severity of coronary artery disease," Nutr. Metab. Cardiovasc. Dis. **19**(3), 211–217 (2009).
14. T.-D. Wang, W.-J. Lee, F.-Y. Shih, C.-H. Huang, W.-J. Chen, Y.-T. Lee, T. T.-F. Shih, and M.-F. Chen, "Association of epicardial adipose tissue with coronary atherosclerosis is region-specific and independent of conventional risk factors and intra-abdominal adiposity," Atherosclerosis **213**(1), 279–287 (2010).
15. A. A. Mahabadi, J. M. Massaro, G. A. Rosito, D. Levy, J. M. Murabito, P. A. Wolf, C. J. O'Donnell, C. S. Fox, and U. Hoffmann, "Association of pericardial fat, intrathoracic fat, and visceral abdominal fat with cardiovascular disease burden: the Framingham Heart Study," Eur. Heart J. **30**(7), 850–856 (2009).
16. G. A. Rosito, J. M. Massaro, U. Hoffmann, F. L. Ruberg, A. A. Mahabadi, R. S. Vasan, C. J. O'Donnell, and C. S. Fox, "Pericardial fat, visceral abdominal fat, cardiovascular disease risk factors, and vascular calcification in a community-based sample: the Framingham Heart Study," Circulation **117**(5), 605–613 (2008).
17. D. M. Jaworski, O. Sideleva, H. M. Stradecki, G. D. Langlois, A. Habibovic, B. Satish, W. G. Tharp, J. Lausier, K. Larock, T. L. Jetton, M. Peshavaria, and R. E. Pratley, "Sexually dimorphic diet-induced insulin resistance in obese tissue inhibitor of metalloproteinase-2 (TIMP-2)-deficient mice," Endocrinology **152**(4), 1300–1313 (2011).
18. S. A. Boppart, W. Luo, D. L. Marks, and K. W. Singletary, "Optical coherence tomography: feasibility for basic research and image-guided surgery of breast cancer," Breast Cancer Res. Treat. **84**(2), 85–97 (2004).
19. C. Zhou, D. W. Cohen, Y. Wang, H.-C. Lee, A. E. Mondelblatt, T.-H. Tsai, A. D. Aguirre, J. G. Fujimoto, and J. L. Connolly, "Integrated optical coherence tomography and microscopy for ex vivo multiscale evaluation of human breast tissues," Cancer Res. **70**(24), 10071–10079 (2010).
20. R. A. McLaughlin, L. Scolaro, P. Robbins, S. Hamza, C. Saunders, and D. D. Sampson, "Imaging of human lymph nodes using optical coherence tomography: potential for staging cancer," Cancer Res. **70**(7), 2579–2584 (2010).
21. A. Ahmad, S. G. Adie, M. Wang, and S. A. Boppart, "Sonification of optical coherence tomography data and images," Opt. Express **18**(10), 9934–9944 (2010).
22. H. Mori, A. D. Borowsky, R. Bhat, C. M. Ghajar, M. Seiki, and M. J. Bissell, "Laser scanning-based tissue autofluorescence/fluorescence imaging (LS-TAFI), a new technique for analysis of microanatomy in whole-mount tissues," Am. J. Pathol. **180**(6), 2249–2256 (2012).
23. Z. Huang, S. Zhuo, J. Chen, R. Chen, and X. Jiang, "Multiphoton microscopic imaging of adipose tissue based on second-harmonic generation and two-photon excited fluorescence," Scanning **30**(6), 452–456 (2008).
24. C. L. Evans, E. O. Potma, M. Puoris'haag, D. Côté, C. P. Lin, and X. S. Xie, "Chemical imaging of tissue *in vivo* with video-rate coherent anti-Stokes Raman scattering microscopy," Proc. Natl. Acad. Sci. U.S.A. **102**(46), 16807–16812 (2005).
25. M.-R. Tsai, S.-Y. Chen, D.-B. Shieh, P.-J. Lou, and C.-K. Sun, "*In vivo* optical virtual biopsy of human oral mucosa with harmonic generation microscopy," Biomed. Opt. Express **2**(8), 2317–2328 (2011).
26. S.-W. Chu, S.-Y. Chen, T.-H. Tsai, T.-M. Liu, C.-Y. Lin, H.-J. Tsai, and C.-K. Sun, "*In vivo* developmental biology study using noninvasive multi-harmonic generation microscopy," Opt. Express **11**(23), 3093–3099 (2003).
27. C.-S. Hsieh, C.-Y. Ko, S.-Y. Chen, T.-M. Liu, J.-S. Wu, C.-H. Hu, and C.-K. Sun, "*In vivo* long-term continuous observation of gene expression in zebrafish embryo nerve systems by using harmonic generation microscopy and morphant technology," J. Biomed. Opt. **13**(6), 064041 (2008).
28. H.-C. Lee, W.-A. Tseng, F.-Y. Lo, T.-M. Liu, and H.-J. Tsai, "*FoxD5* mediates anterior-posterior polarity through upstream modulator Fgf signaling during zebrafish somitogenesis," Dev. Biol. **336**(2), 232–245 (2009).
29. C.-K. Tsai, Y.-S. Chen, P.-C. Wu, T.-Y. Hsieh, H.-W. Liu, C.-Y. Yeh, W.-L. Lin, J.-S. Chia, and T.-M. Liu, "Imaging granularity of leukocytes with third harmonic generation microscopy," Biomed. Opt. Express **3**(9), 2234–2243 (2012).
30. S.-Y. Chen, H.-Y. Wu, and C.-K. Sun, "*In vivo* harmonic generation biopsy of human skin," J. Biomed. Opt. **14**(6), 060505 (2009).
31. S.-Y. Chen, S.-U. Chen, H.-Y. Wu, W.-J. Lee, Y.-H. Liao, and C.-K. Sun, "*In vivo* virtual biopsy of human skin by using noninvasive higher harmonic generation microscopy," IEEE J. Sel. Top. Quantum Electron. **16**(3), 478–492 (2010).
32. C.-K. Chen and T.-M. Liu, "Imaging morphodynamics of human blood cells *in vivo* with video-rate third harmonic generation microscopy," Biomed. Opt. Express **3**(11), 2860–2865 (2012).
33. T. McLaughlin, A. Sherman, P. Tsao, O. Gonzalez, G. Yee, C. Lamendola, G. M. Reaven, and S. W. Cushman, "Enhanced proportion of small adipose cells in insulin-resistant vs insulin-sensitive obese individuals implicates impaired adipogenesis," Diabetologia **50**(8), 1707–1715 (2007).

#177650 - $15.00 USD Received 8 Oct 2012; revised 19 Nov 2012; accepted 21 Nov 2012; published 20 Dec 2012

34. A. Liu, A. Sonmez, G. Yee, M. Bazuine, M. Arroyo, A. Sherman, T. McLaughlin, G. Reaven, S. Cushman, and P. Tsao, "Differential adipogenic and inflammatory properties of small adipocytes in Zucker Obese and Lean rats," Diab. Vasc. Dis. Res. **7**(4), 311–318 (2010).

1. Introduction

Obesity is characterized by excessive body fat mass, which is mostly stored in white adipose tissues in an organism [1–3]. The accumulation of fat, particularly in the visceral adipose tissues, may enhance the risk of diabetes and cardiovascular complications [4–12]. Recently, the increased amount of epicardial adipose tissue, one of the visceral fat depots, has been recognized as a mediator for obesity-related cardiac complications. Patients with increased thickness and volume of epicardial adipose tissues have increased severity of coronary atherosclerosis and risk of future coronary artery disease (CAD) [13–17]. In this context, it is of interest to examine whether the geometric properties of epicardial adipocytes are associated with any pathophysiological significance.

In order to obtain the histological information of adipocytes, researchers have traditionally used bright-field microscopy to inspect the sectioned adipose tissues with fixation and staining. However, sectioning and staining of tissue specimens have some disadvantages like elaborative slide preparation, shape distortion of tissue integrity, and incomplete cellular volume. Besides, the dimensions of human adipocytes are generally in the range of 60-100 μm, which is much larger than the thickness of tissue sections (5-10 μm). Therefore, adipocytes on a slide might not be displayed at their largest cross-sectional area [17]. Consequently, information like size distribution cannot be assessed precisely. To quickly acquire sectioning microscopic images without destroying the structures of intact tissues, investigators often adopt optical tomographic tools like optical coherence tomography (OCT) or confocal laser scanning microscopy. The OCT images typically have deep (2-3 mm) imaging depth with 5-10 μm transverse resolution. The observation of adipose tissues with OCT can roughly display the honeycomb textures on the vertical cross section of biological tissues [18–21]. However, the boundaries are vague for small-sized adipocytes stacked among large ones due to limited resolution and contrast. With the help of fluorescence confocal microscopy, three-dimensional (3D) resolution of adipocyte images can be greatly improved [22]. Multiphoton nonlinear microscopy can achieve deeper imaging depth, while maintaining high 3D resolution [23,24]. Adipocytes with dimensions smaller than 20 μm can thus be clearly visualized. With these advanced microscopy techniques [18–24], we can characterize the 3D morphology of adipocytes without labeling.

Among all label-free optical tomography techniques, third harmonic generation (THG) microscopy can achieve better contrast and transverse resolution (~500 nm) [25] than OCT. Excited by 1230 nm infrared femtosecond laser, THG microscopy has greater imaging depth (~1 mm [26]) than single-photon fluorescence confocal microscopy. The cellular morphologies and subcellular vesicles of embryonic stem cells [26], apoptoic cells [27], somite cells [28], and leukocytes [29] can be clearly observed and real-time tracked with THG microscopy *in vivo*. Compared with two-photon fluorescence microscopy using a Ti:sapphire laser, THG microscopy has less on-focus damage and has been applied in clinical studies for deep tissue and blood cell imaging [25,30–32]. Given these advantages, we herein utilized THG microscopy to directly examine morphologic features of adipocytes in epicardial adipose tissues with submicron 3D spatial resolution. Boundaries and nuclei of adipocytes can be clearly displayed even for small-sized adipocytes. In this preliminary investigation, we, for the first time, found that the size variation of epicardial adipocytes was relatively small in patients with no cardiovascular risk factors undergoing valve surgery, whereas a scattered distribution of adipocyte sizes was noted in patients with CAD undergoing bypass surgery.

#177650 - $15.00 USD Received 8 Oct 2012; revised 19 Nov 2012; accepted 21 Nov 2012; published 20 Dec 2012

2. Materials and methods

2.1. Collection and preparation of adipose tissues for third harmonic generation microscopy

All adipose tissues were obtained from patients undergoing elective cardiac surgery who were enrolled in the research project of National Taiwan University Hospital (Research Ethics Committee of National Taiwan University Hospital: 200812090R). Patients with CAD underwent coronary bypass grafting, whereas patients with no cardiovascular risk factors or DM underwent valve replacement surgery. Both mediastinal and epicardial adipose tissues were excised from the outer surface of the pericardium and the surface of right ventricular free wall, respectively. After removal of visible vessels and fibrous tissue, these adipose tissues were rinsed with phosphate-buffered saline, cut to the appropriate size (2 × 2 mm), and placed directly on slides for THG microscopic examination. The slide has a holding well with 0.3 mm in depth to reduce the stress the cover slip exerted on the tissues and to avoid crushing the structures of samples.

2.2. Oil red O and DAPI staining

To assess the histological features of adipose tissues, Oil Red O and DAPI were used to stain the lipid droplets and nuclei of adipocytes in tissue sections, respectively. Excised adipose tissues were first rinsed with phosphate-buffered saline and then fixed with 4% formaldehyde (Sigma F8775) for 30 min. After sectioning, the tissue sample was treated with 0.1% triton X-100 in phosphate-buffered saline for 5 min and then incubated with Oil Red O solution (Sigma O0625, Sigma 134368) for 3 hours. Finally, it was incubated with DAPI (Sigma B2883) for 30 min.

2.3. Harmonic generation microscopy system for THG microscopy

A harmonic generation microscope was used to obtain the THG (~410 nm) images of adipose tissues. The microscope system includes a femtosecond Cr:forsterite laser (λ = 1230 nm), a scanning unit (FV300, Olympus), an upright optical microscope, a 2D translation stage, photomultiplier tubes (PMTs), a data acquisition card, and imaging reconstruction software. The femtosecond laser typically has 500 mW output power, a pulse repetition rate of 110 MHz, a bandwidth of 38 nm, and a 100 fs pulse width. The laser beam was two-dimensionally scanned by a pair of galvanometer mirrors. Passing the 665-nm-edged dichroic beam splitter, the scanned laser beam was focused by a water immersion NA = 1.0 objective (HCX APO L 20 × 1.00W, Leica, Germany) onto prepared adipose tissues mounted with slides. The power level after the objective was 70 mW, which is well below the damage threshold of human skin [30,31]. Other than THG, second harmonic generation (SHG) signals were generated from collagens. These nonlinear optical signals were epicollected by the same objective, reflected by a 665-nm-edged dichroic beam splitter, further separated by 490-nm-edged dichroic beam splitter, passed the corresponding bandpass filters, and detected separately by two PMTs. The 1024 × 1024 pixel images were sampled by a data acquisition card and reconstructed by image acquisition software. The image frame rate was 3 Hz and three frames were taken for improving signal to noise ratio. The corresponding pixel dwell time was 320 ns. All the samples were imaged at room temperature.

3. Results

3.1. Single-photon fluorescence and THG tomography of adipose tissues

To establish a preliminary understanding on the morphology of adipocytes in fat tissues, we observed cryosectioned mediastinal and epicardial adipose tissues under an inverted fluorescence microscope (Axiovert 100TV, Zeiss). Staining with DAPI and Oil Red O was performed to show the distribution of nuclei and lipid droplets in adipocytes, respectively. The excitation wavelength was 365 nm for DAPI and 546 nm for Oil Red O. Under differential

#177650 - $15.00 USD Received 8 Oct 2012; revised 19 Nov 2012; accepted 21 Nov 2012; published 20 Dec 2012

interference contrast (DIC) microscopy [Fig. 1(a)], we could see elongated ellipsoids of adipocytes compactly stacked together. Their nuclei were displaced to the periphery of the cells [Figs. 1(b), blue], and lipid droplets occupied most volume of adipocytes [Figs. 1(c) and 1(d), red]. We then used the harmonic generation microscopy system to observe the morphological features of epicardial adipocytes.

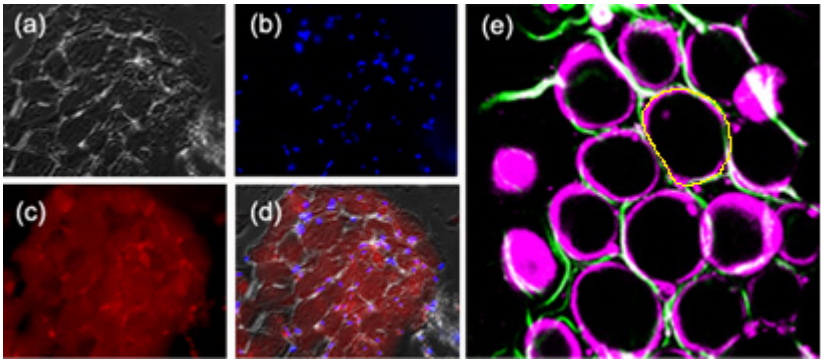

Fig. 1. (a) Differential interference contrast, (b) DAPI staining, and (c) Oil Red O staining images of mediastinal adipose tissue from a patient undergoing cardiac surgery. (d) A superimposition image of (a)-(c). (e) Combined SHG (green) and THG (magenta) images of adipose tissues. The yellow contour represents the boundary of the adipocyte at its largest cross-section. Fields of view: (a)-(d) 445 × 344 μm. (e) 240 × 240 μm. Laser pixel dwell time in (e) was 320 ns.

Typically, THG tomography can reveal the boundaries of adipocytes [Fig. 1(e), magenta]. Their morphologies and sizes were similar to those observed by DIC microscopy. At the periphery of adipocytes, displaced nuclei and cytoplasm have different refractive indices from lipid droplets, which resulted in bright THG contrast. When adipocytes were imaged at their top boundary, normal incidence gave rise to strong interfacial THG in round shapes [Fig. 1(e), left]. In the vicinity of large adipocytes, there were some granular objects (dimension <5 μm), which might be oil droplets secreted from adipocytes. We did not include them in the following analyses of adipocyte morphologies. On the other hand, SHG contrast can reveal the lining of connective collagens [Fig. 1(e), green], which reflects the integrity of biopsied tissues. Theoretically, the axial resolution (sectioning thickness) of THG at 1230 nm is well below 1 μm. Due to tissue aberration and scattering induced wavefront distortion, the axial resolution could be degraded to around 1 μm [24]. To avoid loss of information and to consider the resolution limits, we set axial distance intervals of 1 μm between sectioning images in THG tomography. The penetration depths of THG imaging on adipose tissues were typically more than 200 μm (Fig. 2), which is deep enough to include one to two layers of adipocytes, even for large adipocytes with dimensions of around 100-160 μm. Regarding the image quality, at the imaging depth of 200 μm, the membrane structures of adipocytes could still be seen clearly [Fig. 2(e)].

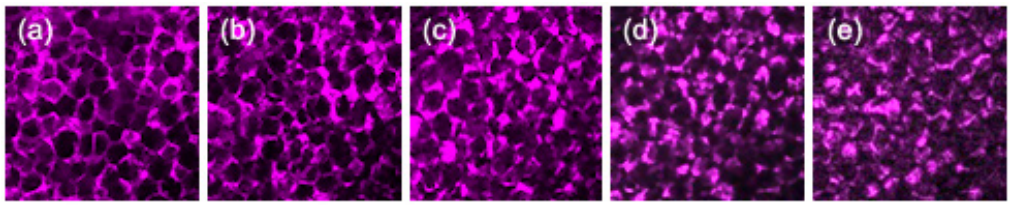

Fig. 2. A THG tomography of adipose tissues at different z-axial distances. The imaging depth of (a) was 80 μm away from the top of tissues. Each section plane was separated by 30 μm in axial distance. Fields of view: 720 × 720 μm. Laser pixel dwell times were 320 ns.

#177650 - $15.00 USD Received 8 Oct 2012; revised 19 Nov 2012; accepted 21 Nov 2012; published 20 Dec 2012

3.2. Morphology of adipocytes in patients with no cardiovascular risk factors and with CAD

Figure 3 shows typical THG sectioning images of adipocytes in epicardial adipose tissues obtained from patients with no cardiovascular risk factors [Fig. 3(a)] and with CAD [Fig. 3(b)]. In tissues of patients with no risk factors, adipocytes looked like well-packed bubbles and had relatively small size variation with dimensions around 70-90 μm. On the contrary, adipocytes in tissues from CAD patients had scattered size distribution [Fig. 3(b)]. Both large-(dimension >120 μm) and small-sized (dimension <40 μm) adipocytes could be seen in the tissues.

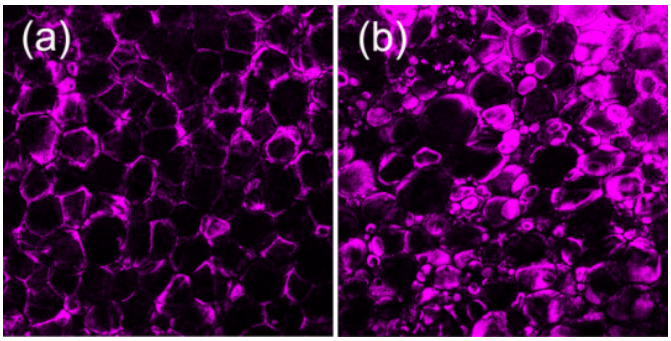

Fig. 3. THG images of adipocytes in epicardial adipose tissue (on the surface of right ventricular free wall) from patients with (a) no cardiovascular risk factors and (b) with CAD. Fields of view: 720 × 720 μm. Laser pixel dwell times were 320 ns.

3.3. Quantitative measures of adipocytes

From sectioning THG images, we measured quantitative parameters at the plane with the largest cross-sectional area for each individual adipocyte. As shown in Fig. 1(e), for the cell to be analyzed, we drew a line along the boundary contour of an adipocyte to measure the corresponding perimeter and enclosed area. To describe the dimension of elliptical adipocytes, we calculated area-equivalent circular diameters (AECD) from enclosed areas. Adipose tissue samples from two patients with no risk factors and two CAD patients were analyzed (Fig. 4). For each case, depending on the quality of samples, the number of adipocytes analyzed was between 270 and 360.

Two patients with no cardiovascular risk factors were treated as control. To evaluate the regional variation of adipocyte sizes, we took adipose tissues from the surface of right ventricle (RV), chest wall, and mediastinum. In each tissue, we chose two to three different locations to acquire THG sectioning images. For RV epicardial adipocytes, their sizes fell within the range of 40-120 μm [Fig. 4(a)]. In the case of first patient [first row in Fig. 4(b)], the average AECD of RV adipocytes was 73 μm. The standard deviation of sizes was 11μm. The number percentage of small-sized adipocytes (AECD < 40 μm) was 2.3%. The relative size variations, which are defined by standard deviation of AECD over average AECD, were 13%, 14%, and 20% at three different locations. The average AECD of RV adipocytes in the other no-risk-factor patient was greater (~86 μm) with a standard deviation of 17 μm [second row in Fig. 4(b)]. The number percentage of small-sized adipocyte was 2%. Their size variations were 18%, 18%, and 20% at three different locations. For non-epicardial adipocytes [Fig. 4(b), Chest and Medi], the average sizes didn't deviate too much from those of RV, with a slightly greater size variations (20-28%).

For two CAD patients without diabetes, a certain amount of small-sized epicardial adipocytes were observed in THG images [Fig. 3(b)]. Their population percentages were raised to 3-7%. Compared with no-risk-factor patients, CAD patients had a broader range of size distribution (20-140 μm) [Fig. 4(c)]. Their standard deviations of size ranged from 20 μm to 29 μm and the relative size variations were 22-33% [Fig. 4(d), RV]. These size variation

#177650 - $15.00 USD Received 8 Oct 2012; revised 19 Nov 2012; accepted 21 Nov 2012; published 20 Dec 2012

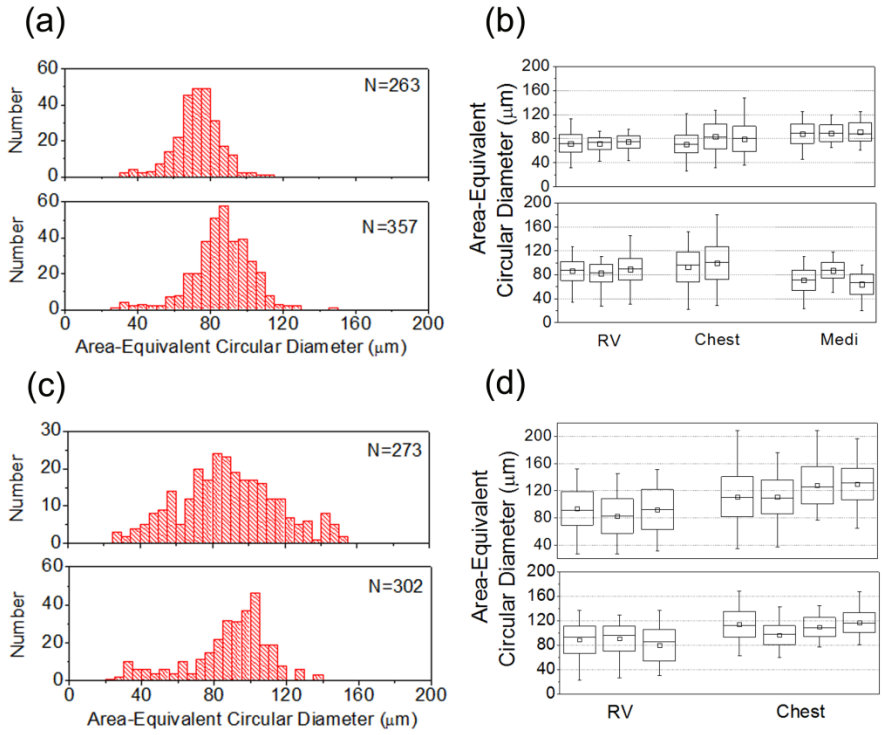

Fig. 4. Histograms and statistics of the sizes (area-equivalent circular diameters) of adipocytes from (a), (b) two patients with no cardiovascular risk factors and (c), (d) three CAD patients. (a), (c) show size histograms of epicardial adipocytes obtained from the surface of right ventricle (RV) and N represents the number of adipocytes analyzed. Box charts (b), (d) illustrate the average (square), median (line in box), variance (box), and ranges of adipocyte sizes measured at different locations within a sample and at different fat tissues in a patient. Adipose tissues were obtained from the surface of right ventricle (RV), subcutaneous tissue of chest wall (Chest), and mediastinal fat (Medi).

parameters were obviously greater than those of epicardial adipocytes in no-risk-factor patients [Fig. 5(a)]. For all CAD patients, the size standard deviations of adipocytes from chest wall were similar to those from RV. There was a similar trend for the perimeter of adipocytes. Patients with CAD had larger standard deviations of perimeters than patients with no cardiovascular risk factors [Fig. 5(b)].

Using perimeter s and area A, we generated another parameter called compression ratio R,

$$R = \frac{A}{\pi\left(s/2\pi\right)^2}, \tag{1}$$

to represent the extent that the adipocytes were compressed. If the adipocyte is of circular shape, this parameter will be 1. In RV epicardial adipose tissues, most of the adipocytes were not severely deformed and their compression ratios were mainly between 0.9 and 1 [Fig. 5(c)].

Using the elongated length a (along long-axis) and the width b of elliptical adipocytes, we also analyzed the eccentricity e of adipocytes as

$$e = \sqrt{1 - \frac{b^2}{a^2}}. \tag{2}$$

#177650 - $15.00 USD Received 8 Oct 2012; revised 19 Nov 2012; accepted 21 Nov 2012; published 20 Dec 2012

For a circle, eccentricity is zero. For an extremely compressed ellipse, the eccentricity will approach 1. This parameter is more sensitive to reflect minute deformation of adipocytes. Again, results showed no significant differences [Fig. 5(d)]. Most of them fell within the range of 0.3 to 0.7 and had mean eccentricities around 0.5.

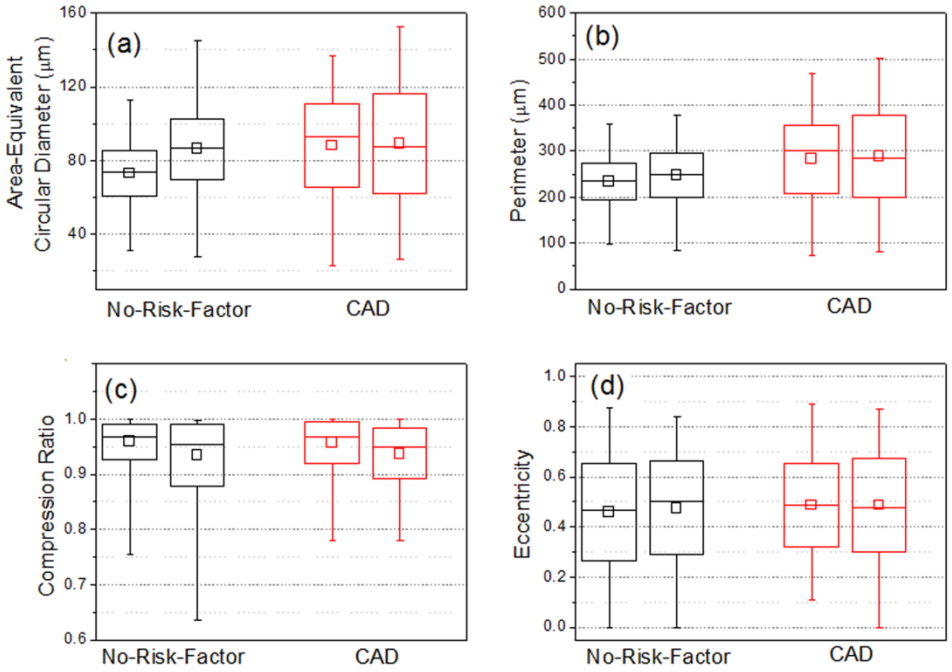

Fig. 5. Statistical results on (a) area-equivalent circular diameter, (b) perimeter, (c) compression ratio, and (d) eccentricity of RV epicardial adipocytes obtained from no-risk-factor (black) and CAD (red) patients.

4. Discussion and conclusion

The preponderance of enlarged visceral adipocytes in obese people has been regarded as a risk factor for future cardiovascular diseases. Using THG tomography on epicardial adipose tissues, we investigated the geometrical properties of adipocytes without fixation or labeling. Intriguingly, we found that not only enlarged, but also a certain amount of small-sized adipocytes existed in epicardial adipose tissues of CAD patients. Recently, it has been shown that small-sized adipocytes had markedly increased pro-inflammatory activity as compared to larger adipocytes in epididymal fat pads of Zucker Obese rats [33,34]. Given that inflammation is one of the fundamental mechanisms of atherogenesis, the identification of a certain amount of small-sized adipocytes in the peri-coronary epicardial adipose tissue might be of pathophysiological significance. However, the validity and clinical significance of this intriguing finding still require further investigation. In summary, these distinctive morphologic features of adipocytes in patients with different pathophysiological backgrounds have not been observed before with traditional histological methods, which might be caused by incomplete size information and loss in the process of preparation, fixation, and labeling. We found epicardial adipocytes in CAD patients have larger standard deviation of area-equivalent circular diameter, larger relative size variation, and higher population percentage of small-sized ones (AECD < 40 μm) than those in no-risk-factor patients. Our results indicate that label-free THG tomography platform can be used to quickly explore the histopathological

#177650 - $15.00 USD Received 8 Oct 2012; revised 19 Nov 2012; accepted 21 Nov 2012; published 20 Dec 2012

features of adipocytes in clinical scenarios based on its superior resolution for virtual optical biopsy.

Acknowledgments

This study is funded by the National Science Council Taiwan under the grant number NSC 100-2628-E-002-006, NSC 101-2314-B-002-192-MY2, and by National Health Research Institutes under the grant number NHRI-EX101-9936EI.

#177650 - $15.00 USD Received 8 Oct 2012; revised 19 Nov 2012; accepted 21 Nov 2012; published 20 Dec 2012